Components of thermal protection mechanism of carbon/phenolic composites exposed to severe aerodynamic heat

Jie Huang[a], Jin Guo[a, b], Haiming Huang[a*], Qing Wang[c], Weijie Li [a]

a. Institute of Engineering Mechanics, Beijing Jiaotong University, Beijing, China;

b. Beijing Key Laboratory of Civil Aircraft Structures and Composite Material, COMAC Beijing Aircraft Technology Research Institute, Beijing, China;

c. Department of Engineering, Durham University, Durham, United Kingdom;

** Corresponding author: huanghaiming@tsinghua.org.cn*

Abstract

In order to improve the thermal protection efficiency of carbon/phenolic (C/Ph) composites used as the heatshield of hypersonic vehicles, it is essential to find out the components of its thermal protection mechanism. In this study, a pyrolysis layer model considering pressure is established to simulate the percentages of heat dissipated by different thermal protection mechanisms. Numerical results reveal that the thermal protection mechanism of C/Ph composites mainly comprises of surface radiation, the heat absorbed by the heat capacity and the TBE of pyrolysis gas, but the TBE weakens as heating time increases. Furthermore, the evolution law of different thermal protection mechanisms of C/Ph composites with resin content is given. Based on the components of thermal protection mechanisms, reducing the thermal conductivity of the resin matrix composites or increasing the material emissivity are effective approaches to enhancing the thermal protection efficiency of C/Ph composites exposed to severe aerodynamic heat.

Keywords: C/Ph composites, Computer modeling, Pyrolysis, Thermal protection mechanism, Efficiency

NOMENCLATURE

Variables

A pre-exponential factor, Hz

c_p specific heat, J/(kg·K)

E Arrhenius law activation energy, J/kg

h enthalpy, J/kg

K permeability coefficient, m^2

k thermal conductivity, W/(m·K)

M mole mass, g/mol

$\dot{m}$ mass injection rate, kg/(m^2·s)

n reaction order

p pressure, Pa

q heat flux, W/m^2

R universal gas constant, J/(mol·K)

T temperature, K

t time, s

u velocity, m/s

x coordinate, m

ΔH enthalpy, J/kg

ε emissivity of material surface

μ dynamic viscosity, Pa·s

ξ porosity

ρ density, kg/m^3

σ Stefan-Boltzmann constant, W/(m^2·K^4)

φ thermal blockage coefficient

Subscripts

c interface between the pyrolysis layer and the char layer

g pyrolysis gases

p interface between the virgin layer and the pyrolysis layer

s solid phase

w material surface

1 the virgin layer

2 the pyrolysis layer

3 the char layer

Abbreviations

C/Ph carbon/phenolic

TBE thermal blockage effect

1. INTRODUCTION

Under aerodynamic heating, various physical and chemical reactions occur in carbon/phenolic (C/Ph) composites exchanging for excellent thermal protection effects [1-3]. The thermal response of C/Ph composites is affected by many factors, such as the heat absorption of resin pyrolysis and the heat dissipation generated by the flow of pyrolysis gas [4-8]. So far, improving the thermal protection efficiency of C/Ph composites used as the heatshield of hypersonic vehicles is still a challenge.

Many scholars have studied the thermal protection mechanism and the thermal response model of thermal protection materials [9-17]. Most thermal response models account for the heat conduction inside the material, the pyrolysis process of the resin matrix, the surface radiation, the flow of pyrolysis gas and the energy transfer caused by the gas flow. For example, Amar [18] presented a study extending the model of polymer matrix composites considering decomposition kinetics, pyrolysis gas flow, and a mixture (solid and gas) energy equation. Chen and Milos [19] developed a series of thermal response programs to simulate the heat conduction, thermal decomposition, flow of pyrolysis gas, and surface ablation of thermal protection system (TPS) materials. Furthermore, Lachaud et al. [20, 21] took a multiscale approach to model and analyze the ablation of porous materials considering the oxidation of a carbon preform and the char layer. The developed model considered the oxygen diffusion through the pores of the materials and in-depth oxidation and mass loss to gain a comprehensive understanding of the ablation process. Based on the model previously developed by Lachaud et al, Martin [22] presented a volume-averaged fiber-scale oxidation model where the mixture energy equation is written as:

$$\frac{d}{dt}\int_{cv}\rho E dV-\int_{cs}\rho h v_{cs}dS+\int_{cs}\phi\rho_g h_g v_g dS+\int_{cs}\dot{q}''dA+\int_{cs}\phi\sum_k J_k h_{gk}dA=0$$

in which the first term accounts for the energy, the second term accounts for the grid

convection, the third term accounts for the gas flux, the fourth term accounts for the heat conduction modeled by the Fourier's Law and the fifth term accounts for the mass diffusion. Recently, Li et al.[23, 24] built physical and mathematical models for the coupling of thermal and ablative responses of material, hypersonic flow response, and chemical response in chemical nonequilibrium boundary layers to explore the influence of gas-phase reactions on the thermal protection performance of charring materials. Based on these thermal protection models, Shi et al. [25-27] found that the main endothermic mechanisms of the silica fiber reinforced polymer composites are radiation, the heat absorption of material and the evaporation of molten fibers. Increasing the heat capacity and emissivity of the thermal protection material is also helpful in improving its heat-absorbing capacity. However, most of the previous studies do not consider the energy dissipated by the pressure change and a discussion of the proportion of different thermal protection mechanisms.

In this paper, a pyrolysis layer model considering pressure is established, the proportion of heat dissipated by each energy dissipation term is predicted, the components of thermal protection mechanism of C/Ph composites exposed to severe aerodynamic heat are analyzed, and a method for improving the thermal protection efficiency of materials is proposed.

2. PYROLYSIS LAYER MODEL CONSIDERING PRESSURE

C/Ph composites are chosen to be widely used as the heatshield of hypersonic vehicles due to their advantages of low density, low thermal conductivity, and heat absorption during high-temperature pyrolysis. Under aerodynamic heating, if the resin matrix starts to pyrolyze, the pyrolysis layer forms. Meanwhile, if the resin matrix totally pyrolyzes, the char layer forms, as shown in Figure 1. These three layers are divided by the pyrolysis degree of resin. On the material surface, aerodynamic heating,

thermal blockage effect (TBE) caused by the injection of pyrolysis gas, surface ablation and combustion of surface char are considered.

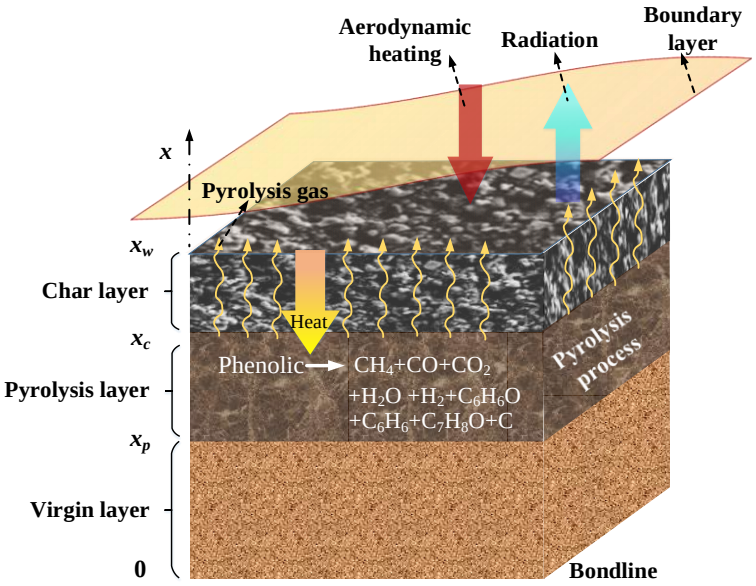

FIGURE 1 The pyrolysis layer model of C/Ph composites

In Figure 1, x is the coordinate along the material thickness, subscripts p and c denote interfaces between these three layers, and subscript w represents the material surface. Furthermore, the pyrolysis process of phenolic resin inside C/Ph composites can be described by four reactions, as presented in Table 1.

Table 1 Pyrolysis equations and kinetic parameters [28]

Reactions	A (s^{-1})	E (J/kg)	n (-)
$PR_1 \rightarrow H_2O$ (physisorbed)	8560	71200	3
$PR_2 \rightarrow 0.69H_2O+0.01C_6H_6+0.01C_7H_8+0.23C_6H_6O$	8560	71200	3
$PR_3 \rightarrow 0.09CO_2+0.33CO+0.58CH_4$	4.98×10^8	170000	3
$PR_4 \rightarrow H_2$	4.98×10^8	170000	3

The mathematical model with pressure for the pyrolysis phenomenon in Figure 1 is established according to the conservation laws of energy, mass and momentum. The governing equations of three different layers are given by

$$\rho_1 c_{p1}\frac{\partial T}{\partial t}=\frac{\partial}{\partial x}\left(k_1\frac{\partial T}{\partial x}\right)+\frac{dp}{dt}-u\xi_g\rho_g c_{pg}\frac{\partial T}{\partial x} \qquad 0\le x<x_p \tag{1}$$

$$\rho_2 c_{p2}\frac{\partial T}{\partial t}=\frac{\partial}{\partial x}\left(k_2\frac{\partial T}{\partial x}\right)+\frac{dp}{dt}-\frac{\partial \rho_s}{\partial t}\left(c_{ps}T-c_{pg}T+\Delta H\right)-u\xi_g\rho_g c_{pg}\frac{\partial T}{\partial x}$$

$$x_p \le x < x_c \tag{2}$$

$$\rho_3 c_{p3}\frac{\partial T}{\partial t}=\frac{\partial}{\partial x}\left(k_3\frac{\partial T}{\partial x}\right)+\frac{dp}{dt}-u\xi_g\rho_g c_{pg}\frac{\partial T}{\partial x} \qquad x_c \le x < x_w \tag{3}$$

in which ρ is the density, c_p is the specific heat, T is the temperature, t is the time, k is the thermal conductivity, p is the pressure, u is the velocity of pyrolysis gas, ξ is the porosity, ΔH is the enthalpy, subscripts 1, 2 and 3 denote the virgin layer, the pyrolysis layer and the char layer respectively, subscript g denotes the pyrolysis gas, and subscript s denotes the solid phase.

The continuity equation of the pyrolysis layer is written as

$$\frac{\partial \xi_g \rho_g}{\partial t}+\frac{\partial}{\partial x}\left(u\xi_g\rho_g\right)=-\frac{\partial \rho_s}{\partial t} \tag{4}$$

In the virgin layer and the char layer, the continuity equation is

$$\frac{\partial\left(\xi_g\rho_g\right)}{\partial t}+\frac{\partial\left(u\xi_g\rho_g\right)}{\partial x}=0 \tag{5}$$

The pyrolysis gas is treated as the ideal gas, and the ideal gas law is

$$p=\frac{\rho_g}{M}RT \tag{6}$$

where M is the mole mass.

As the C/Ph composite is porous, pyrolysis gas flow can be described by the Darcy law

$$u=-\frac{K}{\xi_g\mu}\frac{\partial p}{\partial x} \tag{7}$$

in which K is the permeability coefficient, μ is the dynamic viscosity.

The energy conservative equation at the material surface can be given by

$$-k_3\frac{\partial T}{\partial X}=\varphi q+\frac{\mathrm{d}m_c}{dt}\Delta H_C-\varepsilon\sigma T_w^4 \qquad X=X_w \tag{8}$$

where ε is the emissivity of material surface, φ is the thermal blockage coefficient, σ is the Stefan-Boltzmann constant, and subscript C represents the combustion in material surface.

φ can be defined by the relation

$$\varphi=1-0.58\left(\frac{\mathrm{d}m_{g3}}{dt}+\frac{\mathrm{d}m_c}{dt}\right)\frac{h_r}{q_{cold}} \tag{9}$$

where h_r is the recovery enthalpy, q_{cold} is the cold wall heat flux.

Hot wall heat flux can be given by

$$q=q_{cold}(1-h_w/h_r) \tag{10}$$

where h_w is the wall enthalpy.

The mass injection rate of pyrolysis gas on material surface $\frac{\mathrm{d}m_{g3}}{dt}$ can be given by

$$\frac{\mathrm{d}m_{g3}}{dt}=\xi_g\rho_g u \tag{11}$$

The temperature and the heat flux in $x=x_p$ and $x=x_c$ must satisfy

$$T=T_p \qquad x=x_p \tag{12}$$

$$T=T_c \qquad x=x_c \tag{13}$$

$$-k_1\frac{\partial T(x,t)}{\partial x}=-k_2\frac{\partial T(x,t)}{\partial x} \qquad x=x_p \tag{14}$$

$$-k_2\frac{\partial T(x,t)}{\partial x}=-k_3\frac{\partial T(x,t)}{\partial x} \qquad x=x_c \tag{15}$$

At the material bond line, there are

$$-k_1\frac{\partial T}{\partial x}=0 \qquad x=0 \tag{16}$$

$$\frac{\partial p}{\partial x} = 0 \qquad x = 0 \tag{17}$$

At the material surface, there is

$$p = p_w \qquad x = x_w \tag{18}$$

The initial conditions are

$$T = T_0 \qquad t = 0 \tag{19}$$

$$p = p_0 \qquad t = 0 \tag{20}$$

Specific calculation procedures of the presented pyrolysis layer model considering pressure can be described by the calculation flow chart in Figure 2.

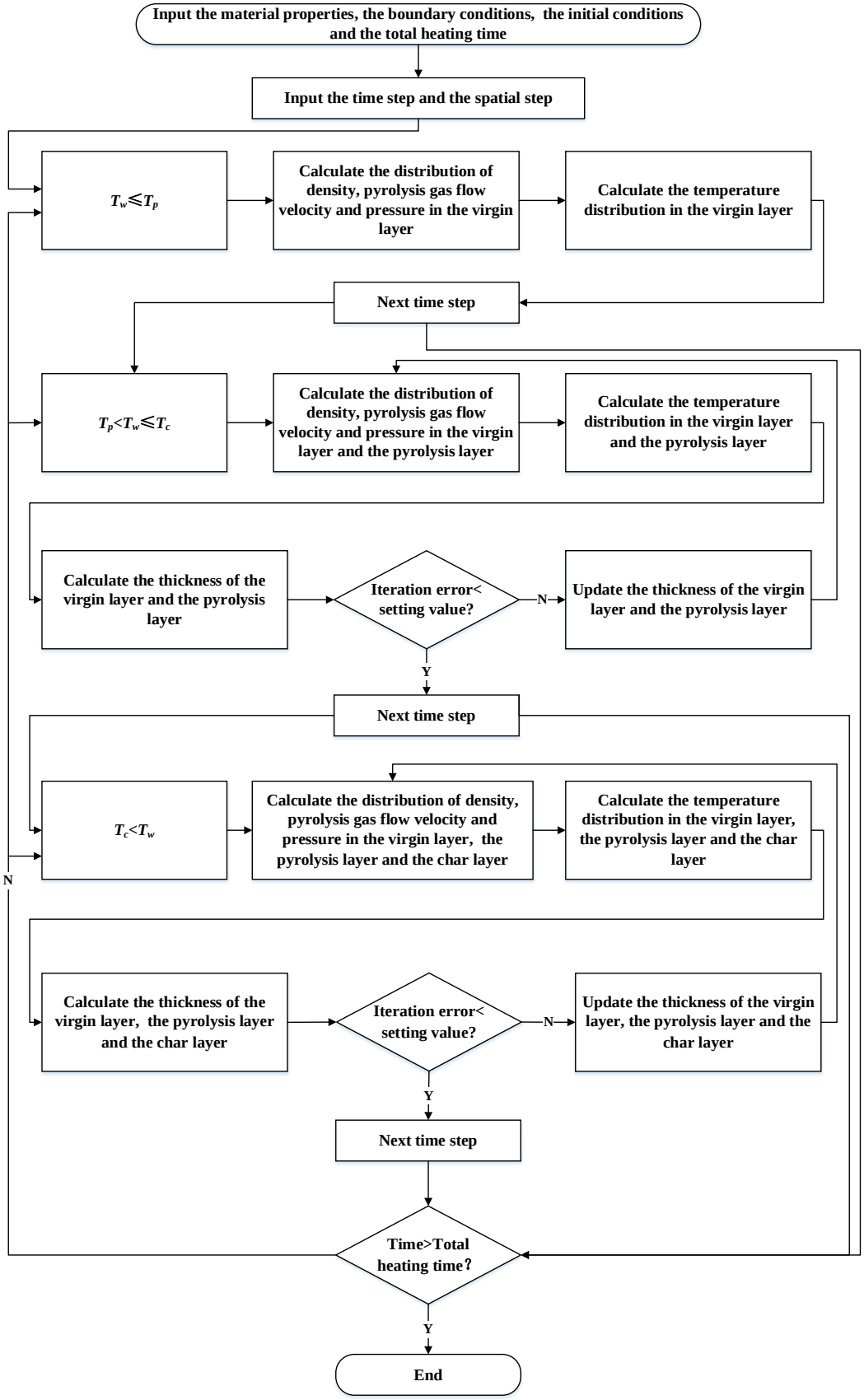

FIGURE 2 Calculation flow chart of the pyrolysis layer model considering pressure

3. COMPONENTS OF THERMAL PROTECTION MECHANISM

Thermal protection efficiency of C/Ph composites is closely related to their thermal protection mechanisms. In this section, the proportions of the thermal protection mechanism of C/Ph composites are given in detail. Besides, the improved method of thermal protection efficiency of C/Ph composites is proposed according to the numerical results.

3.1 Energy dissipation terms in C/Ph composites

There are several ways to dissipate heat on the material surface. For example, TBE caused by the injection of pyrolysis gas is helpful to reduce the heat flux applied on the material surface. Meanwhile, thermal radiation dissipates heat on the material surface from the high temperature region to the lower region. In addition, if the surface temperature is high enough, the carbon on the material surface will be oxidized and this process will release heat. We define:

$$q_{rad} = \varepsilon \sigma T_w^4 \tag{21}$$

$$q_{rzs} = (1-\varphi) q \tag{22}$$

$$q_{in} = -k_3 \frac{\partial T}{\partial x} \tag{23}$$

$$q_{com} = \frac{\mathrm{d}m_c}{dt} \Delta H_c \tag{24}$$

where subscripts *rad*, *rzs*, *in* and *com* stand for the thermal radiation, the TBE, the thermal conduction and the surface carbon combustion, respectively.

Inside C/Ph composites, there are many ways of heat dissipation taken into consideration in the pyrolysis layer model with pressure by different terms. According to the energy conservation equation in each layer, the heat transferred from the high-

temperature region to the interior of the material is mainly dissipated by the following means: (1) The heat capacity absorbs heat; (2) the injection of pyrolysis gas dissipates heat; (3) the change of gas pressure inside the material dissipates heat; (4) the resin pyrolysis dissipates heat (only in the pyrolysis layer). We define:

$$q'_{con} = \frac{\partial q_{con}}{\partial x} = \frac{\partial}{\partial x}\left(k_i \frac{\partial T}{\partial x} \right) \qquad i = 1,2,3 \tag{25}$$

$$q'_{rer} = \frac{\partial q_{rer}}{\partial x} = -\rho_i c_{pi} \frac{\partial T}{\partial t} \qquad i = 1,2,3 \tag{26}$$

$$q'_{pre} = \frac{\partial q_{pre}}{\partial x} = \frac{dp}{dt} \tag{27}$$

$$q'_{pyr} = \frac{\partial q_{pyr}}{\partial x} = -\frac{\partial \rho_s}{\partial t}\left(c_{ps}T - c_{pg}T + \Delta H \right) \tag{28}$$

$$q'_{gf} = \frac{\partial q_{gf}}{\partial x} = -u\xi_g \rho_g c_{pg} \frac{\partial T}{\partial x} \tag{29}$$

where q' stands for heat flow derivation to coordinate, subscripts *con*, *rer*, *pre*, *pyr* and *gf* stand for the thermal conduction, the material heat capacity, the dissipation term of pressure change, the dissipation term of resin pyrolysis and the dissipation term of pyrolysis gas flow, respectively.

3.2 Main thermal protection mechanism of C/Ph composites

In order to estimate the thermal response of C/Ph composites and further analyze the thermal protection mechanism, a specific aerodynamic heating condition is applied in this section. The aerodynamic heating conditions are as follows: the heat flux of the cold wall is 0.2 MW/m^2, the enthalpy is 12 MJ/kg, the air pressure at the wall is 10 kPa, the total aerodynamic heating time is 300s, and the material thickness is 0.05m.

As a typical C/Ph composite, Phenolic impregnated carbon ablator (PICA) is widely used as the heatshield of hypersonic vehicles. The relevant thermophysical parameters of PICA are shown in Table 2.

Table 2 Relevant thermophysical parameters of PICA[29-32]

Properties	Unit	Value	References
ρ_1	kg/m^3	234	[30]
ρ_3	kg/m^3	193	[30]
k_1	W/(m·K)	0.31	[31]
k_3	W/(m·K)	$2.1187\times10^{-4}\times T+0.9907$	[30]
cp_1	J/(kg·K)	$1.6548\times T+817.0709$	[30]
cp_3	J/(kg·K)	$0.0754\times T+4460.6$	[30]
K_1	m^2	1.33×10^{-11}	[32]
K_3	m^2	3.81×10^{-11}	[32]
T_p	K	489	[31]
T_c	K	1089	[29]
ε	-	0.89	[31]
ξ_1	-	80 %	[30]
ξ_3	-	90 %	[30]

The variations of q, q_{rad}, q_{rzs}, q_{in} and q_{com} at $x = x_w$ with time are presented in Figure 3. The heat flux q applied on the surface of C/Ph composites is mainly dissipated by the radiation heat dissipation q_{rad} and the TBE of pyrolysis gas q_{rzs}. The residual heat flux q_{in} enters into the composite by heat conduction. Since the heat flow at $x = x_w$ is small and the surface temperature is low, there is no surface ablation phenomenon at the material surface, that is, $q_{com} = 0$. As can be seen from Figure 3, at $x = x_w$, the heat dissipated by thermal radiation is the largest, followed by the energy dissipated by the TBE of pyrolysis gas. Surface radiation is closely correlated with the surface temperature. As presented in Figure 4, the surface temperature rises rapidly at the beginning, then increases slowly after 50 s and basically stays constant at 1160 K. The heat flux of surface radiation q_{rad} rises rapidly at the beginning of heating, then slows down gradually, and remains basically unchanged thereafter, which is the same as the trend of material surface temperature. The TBE of pyrolysis gas consumes the heat flux q_{rzs} obviously at the initial heating stage, but it decreases gradually under continuous heating. The reason is that the temperature gradient inside the material is high at the initial stage of heating, and a large amount of pyrolysis gas is produced by the intense pyrolysis of the resin. While at the later stage of heating, the temperature gradient inside

the material decreases gradually, and the amount of pyrolysis gas produced by resin pyrolysis reduces gradually. Figure 5 shows the changing trend of the pyrolysis gas mass injection rate with time when $x = x_w$. The variation trend of the TBE of pyrolysis gas is consistent with that of the pyrolysis gas mass injection rate.

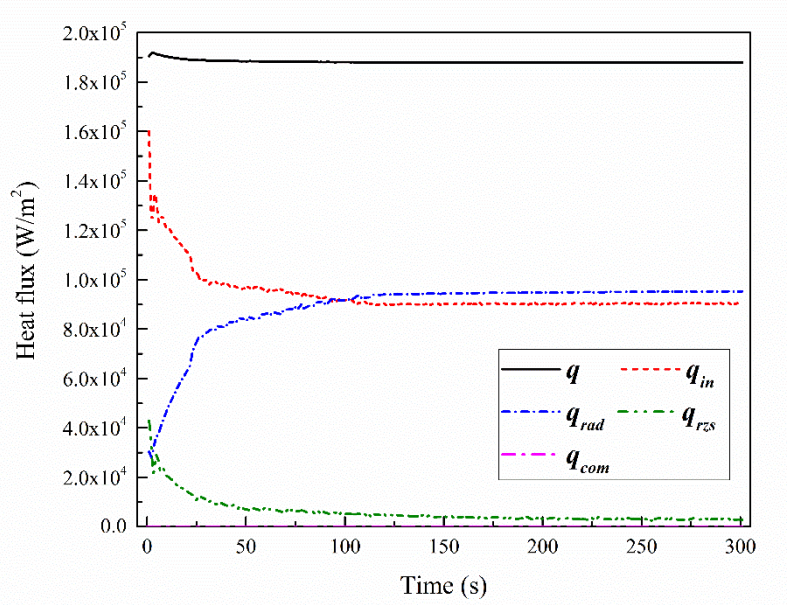

FIGURE 3 Variation histories of q, q_{rad}, q_{rzs}, q_{in}, q_{com} at $x = x_w$

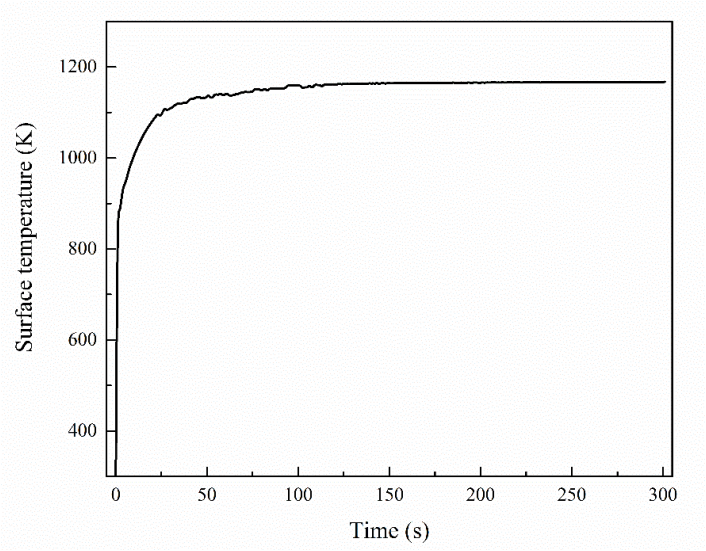

FIGURE 4 Profiles of surface temperature of PICA under aerodynamic heating

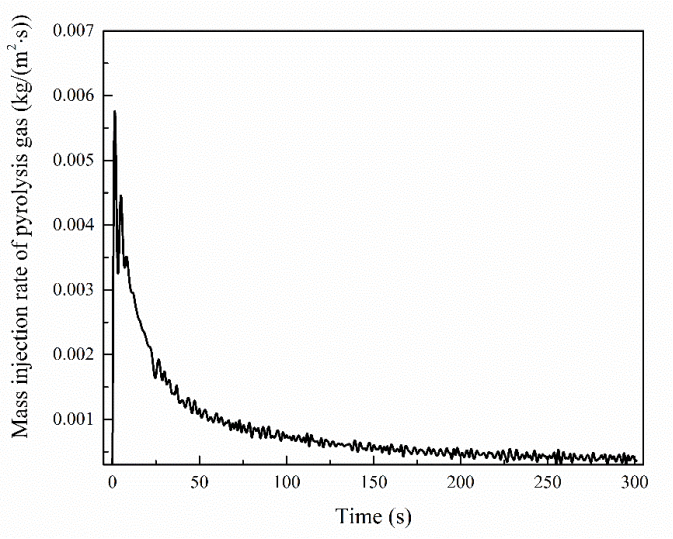

FIGURE 5 Mass injection rate of pyrolysis gas at $x = x_w$

To study the evolution law of the energy dissipation terms at different positions in the PICA material, Figure 6 shows the variations of the q'_{con}, q'_{pyr}, q'_{rer}, q'_{gf} and q'_{pre} at different thicknesses (the distances from the material bond line are 0.045 m, 0.04 m, 0.03 m, 0.02 m and 0.01 m), respectively. The positive value in Figure 6 represents the heat transferred from the high-temperature region per unit volume in unit time while the negative value represents the dissipated heat. With the increase of heating time, the absolute values of q'_{con}, q'_{pyr}, q'_{rer}, q'_{gf} and q'_{pre} at different positions first increase and then decrease. This phenomenon suggests that the different heat transfer processes inside composites are intense at the initial time but weaken as time increases under a constant aerodynamic heating. In Figure 6 (a), the times corresponding to the peak point of the heat conduction are 8 s, 27 s, 88 s, 180 s and 292 s, respectively, that is, the time the resin begins to pyrolyze at this position. This is because the thermal conductivity of the material increases rapidly when the resin begins to pyrolyze to produce carbon residue, then the heat is transferred to the low temperature region quickly. Figure 6 (b) shows the change of q'_{pyr} at different positions of C/Ph composites. It is found that the closer it is to the surface of the material, the greater the heat dissipated by the resin

pyrolysis. This is because the temperature gradient near the material surface is significantly larger than that near the bond line of the material. The larger the temperature gradient, the faster the pyrolysis rate of the resin and the more heat dissipation of the resin pyrolysis occurs. Figure 6 (c) shows the variation of the endothermic term of heat capacity q'_{rer} at different positions. It shows the same tendency of the changing trend of the heat conduction term q'_{con} since the heat absorbed by the material heat capacity is closely related to that conducted from the high-temperature region. As shown in Figure 6 (d), there are slight oscillations in the endothermic term of pyrolysis gas flow q'_{gf} at different positions, which is caused by the oscillation of the mass injection rate. It is observed in Figure 5 that the mass injection rate of pyrolysis gas fluctuates. Similarly, the endothermic term q'_{pre} oscillates at different thicknesses, as shown in Figure 6 (e). This is caused by the oscillation of in-depth pressure distribution.

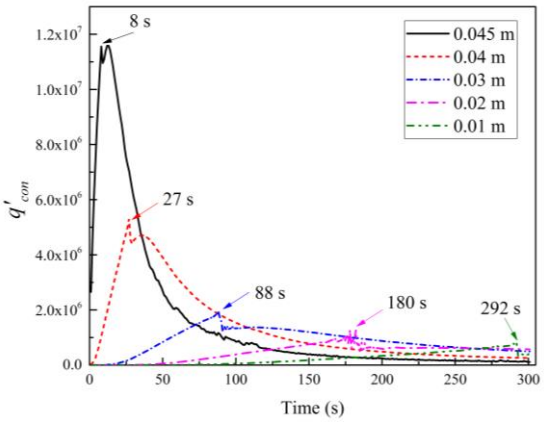

(a)

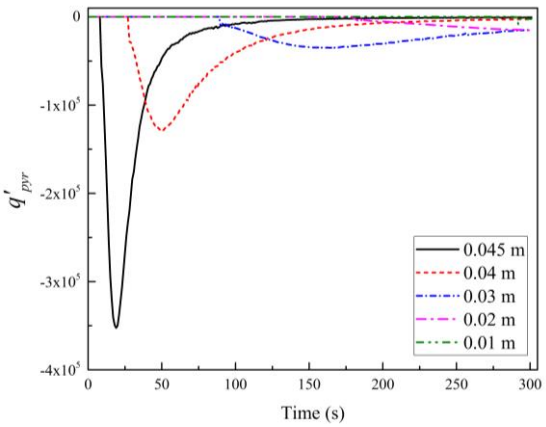

(b)

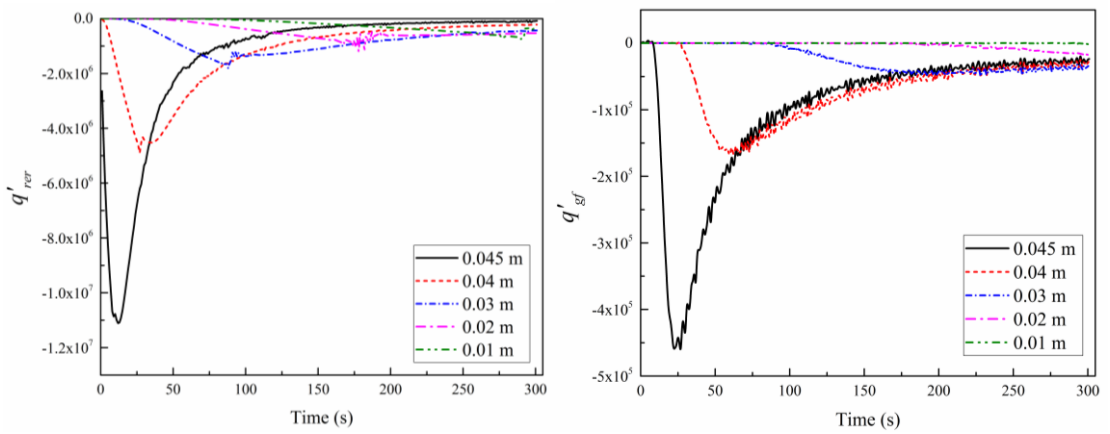

(c) (d)

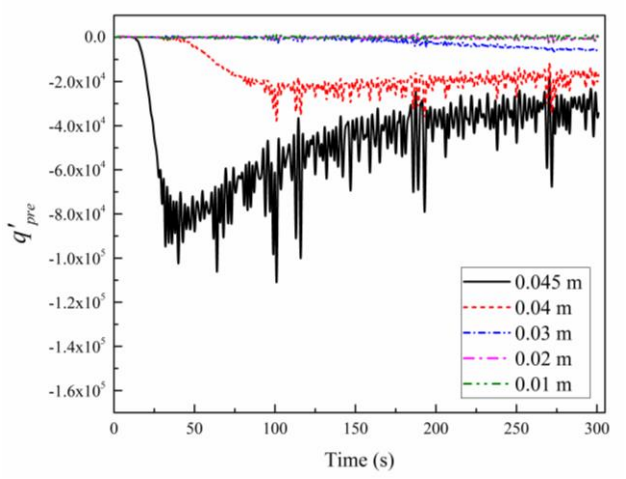

(e)

FIGURE 6 Distribution profiles of physical quantities at different locations in PICA material vary with time: (a) q'_{con}, (b) q'_{pyr}, (c) q'_{rer}, (d) q'_{gf} and (e) q'_{pre}

In order to analyze the main heat dissipation modes and their influencing factors in the material, the heat flux on the material surface is integrated in time, and the heat dissipation items inside the material are integrated in time and space.

$$\psi_{tot} = \int_{t=0}^{t=time} q dt \tag{30}$$

$$\psi_{rad} = \int_{t=0}^{t=time} q_{rad} dt \tag{31}$$

$$\psi_{rzs} = \int_{t=0}^{t=time} q_{rzs} dt \tag{32}$$

$$\psi_{in} = \int_{t=0}^{t=time} q_{in} dt \tag{33}$$

$$\psi_{rer} = \int_{t=0}^{t=time} \int_{x=0}^{x=L} q'_{rer} dxdt \tag{34}$$

$$\psi_{pre} = \int_{t=0}^{t=time} \int_{x=0}^{x=L} q'_{pre} dxdt \tag{35}$$

$$\psi_{pyr} = \int_{t=0}^{t=time} \int_{x=0}^{x=L} q'_{pyr} dxdt \tag{36}$$

$$\psi_{gf} = \int_{t=0}^{t=time} \int_{x=0}^{x=L} q'_{gf} dxdt \tag{37}$$

where Ψ stands for the heat per unit area and subscript *tot* stands for the total heat.

Meanwhile, in order to quantitatively study the percentage of each energy dissipation term on the surface and inside of the material in the whole heating process, percentages of Ψ_{rad}, Ψ_{rzs}, Ψ_{in}, Ψ_{rer}, Ψ_{pre}, Ψ_{pyr} and Ψ_{gf} in Ψ_{tot} are calculated using the following formulae:

$$bfb_{rad} = \psi_{rad} / \psi_{tot} \tag{38}$$

$$bfb_{rzs} = \psi_{rzs} / \psi_{tot} \tag{39}$$

$$bfb_{in} = \psi_{in} / \psi_{tot} \tag{40}$$

$$bfb_{rer} = \psi_{rer} / \psi_{tot} \tag{41}$$

$$bfb_{pre} = \psi_{pre} / \psi_{tot} \tag{42}$$

$$bfb_{pyr} = \psi_{pyr} / \psi_{tot} \tag{43}$$

$$bfb_{gf} = \psi_{gf} / \psi_{tot} \tag{44}$$

where *bfb* stands for the percentage.

Figure 7 shows the percentage of the energy dissipation terms Ψ_{rad}, Ψ_{rzs}, Ψ_{rer}, Ψ_{pyr}, Ψ_{pre} and Ψ_{gf} in the total heat Ψ_{tot} of PICA. It is illustrated that the heat consumed by thermal radiation accounts for 46.29% of the whole heating process under the given

boundary condition, which has a crucial impact on the thermal protection performance of materials. This is because the surface emissivity of PICA is high, and the surface emissivity further increases when the char layer forms on the surface. Moreover, due to the small resin content and low weight loss of PICA material, the amount of pyrolysis gas generated by resin pyrolysis is small. Therefore, the TBE of pyrolysis gas is not significant, and its heat consumption accounts for 3.05 % of the total heat. It is observed in Figure 7 that the heat entering the material is not only absorbed by the heat capacity of the material itself, but also dissipated through the heat absorption of resin pyrolysis, pyrolysis gas flow and pressure change. The results show that the main means of heat dissipation of PICA are heat capacity absorption (48.87%), surface radiation (46.29%), TBE of pyrolysis gas (3.05%), pyrolysis gas flow (0.86%), pressure change (0.6%) and resin pyrolysis absorption (0.33%). Since the resin mass fraction of PICA is small, heat dissipated by pyrolysis gas flow, pressure change and resin pyrolysis absorption can be neglected.

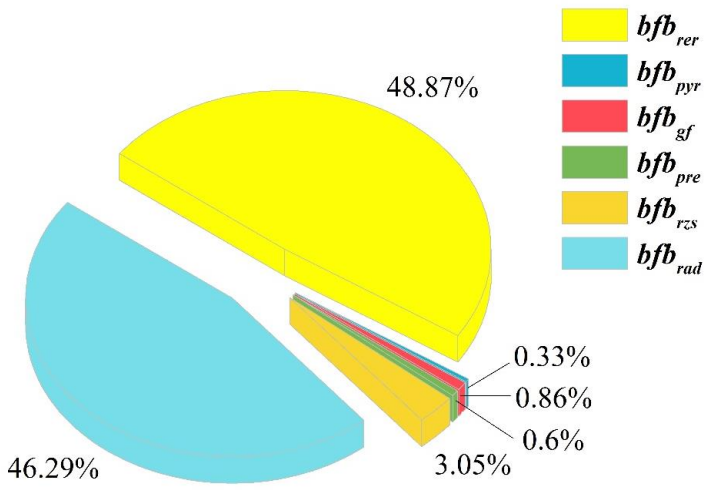

FIGURE 7 Percentage of Ψ_{rad}, Ψ_{rzs}, Ψ_{rer}, Ψ_{pyr}, Ψ_{pre}, Ψ_{gf} of PICA

Based on the above analysis results, the following methods can be adopted to improve the thermal protection efficiency of low-density C/Ph composites: (1) The surface of C/Ph composites can be treated or coated to make it have a higher radiation

coefficient, therefore, the radiation heat dissipation of the material surface is enhanced. (2) Fiber with a larger specific heat capacity can be selected as the preform of the composites, such as carbon fiber and silicon dioxide fiber, to increase the heat absorption capacity of the material. (3) Reducing the thermal conductivity of the composite is an effective method to increase the surface radiation heat dissipation. For example, the matrix of the composites can be fabricated as the phenolic aerogel, which reduces the thermal conductivity of the composites through the micro-pore structure.

3.3 Influence of resin content on thermal protection mechanism of C/Ph composites

For the purpose of studying the influence of resin content on the thermal protection mechanism of C/Ph composites, the aerodynamic heating conditions are chosen to be the same as those in section 3.1, but the resin mass fraction rises from 30% to 50%. Material thickness is 0.03 m and density of carbon fiber preform is 160 kg/m^3. Relevant material properties of C/Ph composites with different resin mass fractions are shown in Table 3.

Table 3 Properties of C/Ph composites with different resin mass fractions

Resin mass fraction (-)	Density of the virgin layer (kg/m^3)	Density of the char layer (kg/m^3)	Density of the fiber reinforcement (kg/m^3)
30 %	229	194	160
35 %	246	194	160
40 %	267	194	160
45 %	291	194	160
50 %	320	194	160

Figure 8 shows the variation rule of bfb_{rzs} of C/Ph composites surface in different time periods when the resin content is 30%. It is found that the TBE of pyrolysis gas on the material surface has a time effect. When the aerodynamic heating time increases, bfb_{rzs} gradually decreases, but its downward trend slows down. At the same time, pie charts show the percentage of each energy dissipation term on the material surface. The

percentage of heat dissipated by thermal radiation at the material surface of the total heat, bfb_{rad}, increases obviously with time, which is 24.93% within 20 s, and increases to 47.09% within 300 s. This is caused by the increase of material surface temperature. The higher the temperature is, the greater the total radiated energy is. Correspondingly, as time increases, bfb_{in} presents a continuous downward trend, which is 63.84% in 20 s and decreases to 49.81% in 300 s.

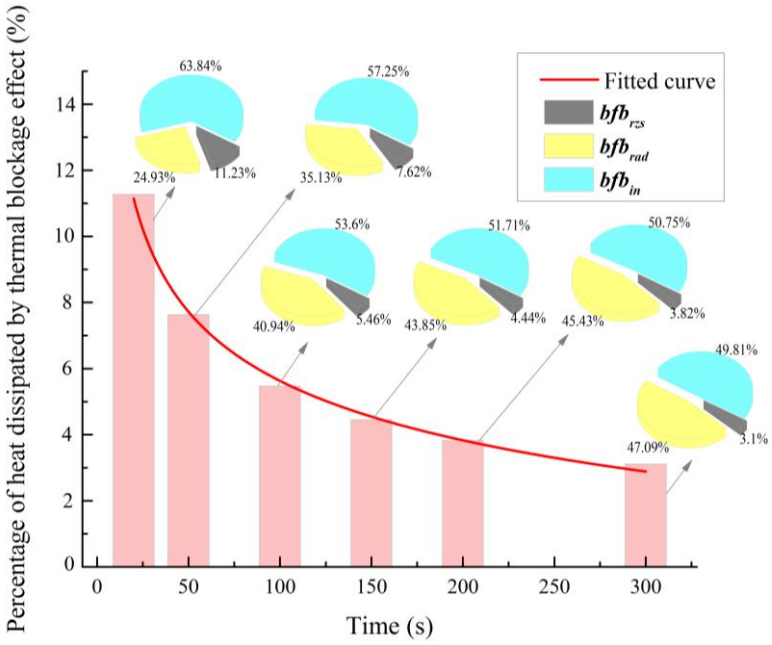

FIGURE 8 Variation of different energy dissipation terms at different times

Because of the time effect of the TBE of pyrolysis gas, the percentage of each energy dissipation term on the material surface is diverse in different time periods. Therefore, numerical results of different resin mass fractions in 100 s periods are taken for discussion. Figure 9 shows the evolution law of the percentage of each energy dissipation term at the surface of C/Ph composites with different resin mass fractions in 100 s. Corresponding to different resin mass fractions, the surface radiation of C/Ph composites is one of the main ways of heat dissipation, and the heat dissipated by surface radiation is much greater than that dissipated by the TBE of pyrolysis gas on the material surface. However, the percentage of heat dissipated by the TBE of pyrolysis

gas of the total heat increases gradually as the resin mass fraction of C/Ph composites rises. When the resin mass fraction increases from 30% to 50%, the bfb_{rzs} increases from 5.46% to 14.03 %. The relationship between bfb_{rzs} and the resin mass fraction is approximately linear. By contrast, the percentage of heat dissipated by thermal radiation on the material surface decreases gradually as the resin mass fraction rises. When the mass fraction of the resin goes from 30% to 50%, the bfb_{rad} decreases from 40.94% to 35.53%, which is due to the declination of surface temperature.

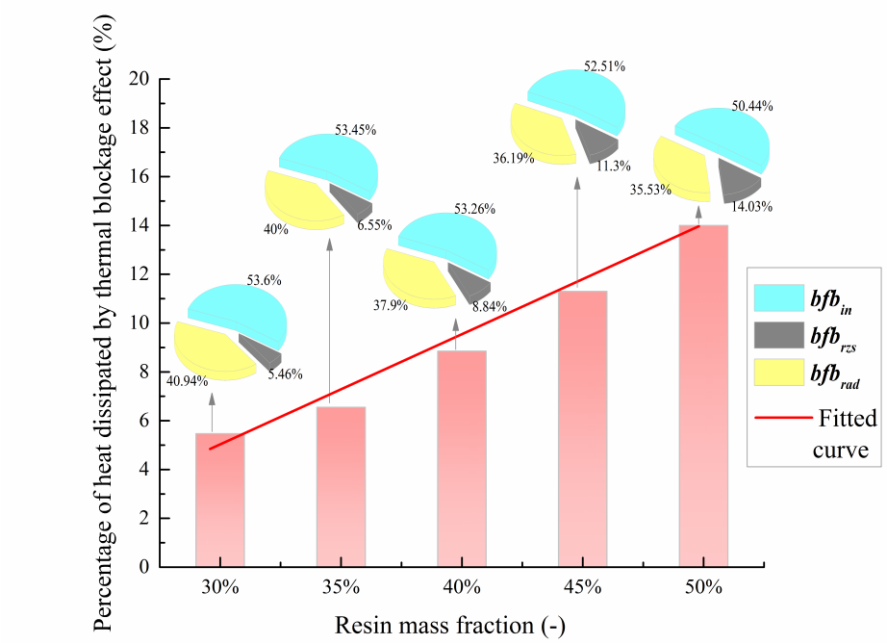

FIGURE 9 Percentages of Ψ_{rad}, Ψ_{rzs}, Ψ_{in} with different mass fraction of resin

Figure 10 presents the surface temperature distribution curve of the C/Ph composites with different resin mass fractions. As shown in Figure 10, the more resin content of the material, the lower the surface temperature. The decrease of temperature is caused by the increase of the amount of generated pyrolysis gas, and the TBE of pyrolysis gas on the material surface is more and more apparent, which effectively blocks the aerodynamic heating. Finally, the proportion of heat entering the material in the total heat bfb_{in} shows a downward trend along with the mass fraction of resin increase. As the mass fraction of the resin goes from 30% to 50%, bfb_{in} decreases from

53.6% to 50.44%. However, composite density increases with the rising of resin mass fraction, which is against the optimal design of the TPS. Furthermore, a rise in the resin mass fraction directly results in the declination of heat dissipated by surface radiation. Therefore, the method of increasing the resin mass fraction to enhance the thermal protection efficiency of C/Ph composites is not suggested in practical engineering applications.

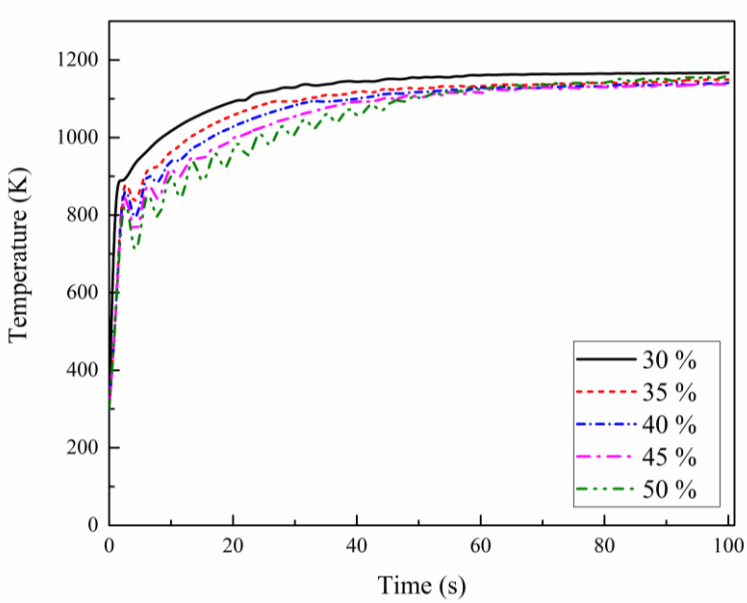

FIGURE 10 Surface temperature profiles of material with different resin mass fractions

3.4 Improved method of thermal protection efficiency of C/Ph composites

From the above analysis, it can be seen that there is a competitive mechanism between the heat dissipated by surface radiation and the heat dissipated by the TBE of pyrolysis gas, that is, if the TBE of pyrolysis gas is enhanced, the surface temperature can be reduced, but leading to the decrease of heat dissipated by surface radiation. Enhancing the heat dissipation of TBE of pyrolysis gas or enhancing the heat dissipation of surface radiation can effectively reduce the heat entering the material, but to enhance the TBE of pyrolysis gas requires an increase the mass flow rate of pyrolysis gas in the material. Although the mass flow rate of pyrolysis gas can be significantly

increased by enhancing the mass fraction of the resin in the material, the density of materials is also obviously increased, which is not conducive to the optimization design of TPS of the aircraft. The approach to enhancing the thermal protection efficiency of C/Ph composites is suggested in the following ways: (1) Reduce the thermal conductivity of the resin matrix composites. The resin matrix composites with low thermal conductivity can effectively block the heat transferring to the back of the material, thus significantly increasing the surface temperature and reducing the temperature rise at the back of the material. The heat radiated in the material surface is significantly enhanced. (2) Increase the emissivity of the material surface, such as applying a high emissivity coating on the material surface or surface ceramic treatment of resin-based composites.

4. CONCLUSIONS

For the purpose of improving the thermal protection efficiency of C/Ph composites, a pyrolysis layer model considering pressure is established and then the components of a thermal protection mechanism of the composites exposed to severe aerodynamic heating are analyzed. The thermal protection mechanism is given and the method for improving the thermal protection efficiency is proposed.

The thermal protection mechanism of C/Ph composites is mainly composed of the thermal radiation on the surface, the absorption heat of material heat capacity and TBE of pyrolysis gas. At the same time, the TBE of pyrolysis gas has a time effect, that is, the TBE is evident in the case of short-time aerodynamic heating. As heating time increases, the TBE becomes less and less noticeable. In brief, there is a competitive mechanism between the surface radiation and endothermic terms caused by resin matrix pyrolysis, pyrolysis gas flow and TBE of pyrolysis gas.

The methods for improving the thermal protection efficiency of materials are

proposed based on the above competitive mechanism. Firstly, increasing the surface radiation is suggested rather than increasing the resin content of C/Ph composites. Secondly, reducing the thermal conductivity of materials at high temperatures is also a good approach, which can not only increase the surface radiation but also improve the thermal insulation performance.

ACKNOWLEDGMENT

This work was supported by the National Natural Science Foundation of China [grant number 11772042] and Project funded by China Postdoctoral Science Foundation [grant number 2022M713452].

CONFLICT OF INTEREST

We wish to confirm that there are no known conflicts of interest associated with this publication and there has been no significant financial support for this work that could have influenced its outcome.

REFERENCES

[1] M. Natali, I. Puri, J.M. Kenny, L. Torre, M. Rallini, *Polym. Degrad. Stabil*, **2017**, 141:84-96. https://doi.org/10.1016/j.polymdegradstab.2017.05.017

[2] W.J. Li, H.M. Huang, B.C. Ai, Z.M. Zhang, *Appl. Therm. Eng.* **2016**, 93, 849-855. https://doi.org/10.1016/j.applthermaleng.2015.10.070

[3] Y.K. Chen, F.S. Milos, *J. Spacecraft Rockets* **2013**, 50(2), 256-269. https://doi.org/10.2514/1.A32289

[4] S. Meng, Y. Zhou, W. Xie, F. Yi, S. Du, *J. Spacecraft Rockets* **2016,** 53(5),1-6. https://doi.org/10.2514/1.A33612

[5] F.S. Milos, M. Gasch, *53rd AIAA Aerospace Science Meeting*, Kissimmee, Florida, **2015**.

[6] J. Guo, H. M. Huang, Q. Wang, Y. Zhao, *Polym. Degrad. Stabil*. **2019**, 166, 155-162. https://doi.org/ 10.1016/j.polymdegradstab.2019.05.035

[7] F. Yang, W.H. Xie, S.H. Meng, *Int. J. Mech. Sci.* **2020**, 187, 106110. https://doi.org/10.1016/j.ijmecsci.2020.106110

[8] J. Guo, J. Huang, H.M. Huang, W.J. Li, *Acta Astronaut.* **2020**, 171, 352-358. https://doi.org/10.1016/j.actaastro.2020.03.020

[9] F.S. Milos, Y.K. Chen, *J. Spacecraft Rockets* **2009**, 46(6), 1089-1099. https://doi.org/10.2514/1.36575

[10] H. Zhang, L. Yan, S. Zhou, H. Zou, X. Ren, *Polym. Eng. Sci.* **2020**. https://doi.org/10.1002/pen.25587

[11] Y.X. Zhang, B.L. Wang, Y.L. Shang, 4th International Workshop on Renewable Energy and Development, Electr Network, **2020**. https://doi.org/ 10.1088/1755-1315/510/5/052038

[12] S.B. Shi, B. Lei, M.Y. Li, X.F. Cui, X.B. Wang, X.B. Wang, S. Tang, J.J. Shen, *Prog. Org. Coat.* **2020**, 143, 105609. https://doi.org/10.1016/j.porgcoat.2020.105609

[13] Y.S. Meng, L. Yan, W. Huang, C. Ji, J. Li, *Aerosp. Sci. Technol.* **2021**, 115, 106840. https://doi.org/10.1016 /j.ast.2021.106840

[14] J. Huang, W.X. Yao, *Int. J. Heat Mass Tran.* **2021**, 152, 119549. https://doi.org/10.1016/j.ijheatmasstransfer.2020. 119549

[15] C.B. Moyer, R.A. Rindal, NASA technical report, **1968**:NASA CR-1061.

[16] K.A. Trick, T.E. Saliba, S.S. Sandhu, *Carbon* **1997**, 35(3), 393-401. https://doi.org /10.1016/S0008-6223(97)89610-8

[17] W.H. Xie, Y.J. Yang, S.H. Meng. *J. Spacecr. Rockets.* **2019**, 56(6), 1765-1774. https://doi.org/10.2514/1.A34392

[18] A.J. Amar, Raleigh: North Carolina State University, **2006**.

[19] Y.K. Chen, F.S. Milos, *J. Spacecraft Rockets* **2018**, 55(4), 914-927. https://doi.org/10.2514/1.A34184

[20] J. Lachaud, Y. Aspa, G.L. Vignoles G L, *Int. J. Heat Mass Tran.* **2008**, 51(9-10): 2614-2627. https://doi.org/10.1016/j.ijheatmasstransfer.2008.01.008

[21] J. Lachaud, I. Cozmuta, N.N. Mansour, J. Spacecr. Rockets. 2010,47(6): p.910-921. https://doi.org/10.2514/1.42681

[22] A. Martin, *the 44th AIAA Thermophysics Conference*. San Diego, **2013**. https://doi.org/10.2514/6.2013-2497

[23] W. Li, J. Huang, Z. Zhang, H. Huang, J. Liang, *Polym. Composite.* **2020**, 41(7). https://doi.org/10.1002/pc.25571

[24] W. Li, J. Huang, Z. Zhang, H. Huang, Li Wang, *Polym. Composite*. **2020,** 41(12). https://doi.org/10.1002/pc.25773

[25] S.B. Shi, Y. Chen, C.X. Dai, J. Liang, *Thin Wall Struct.* **2021**, 164, 107742. https://doi.org/10.1016/ j.tws.2021.107742

[26] S.B. Shi, Y.F. Wang, Y. Li, *Compos. Struct.* **2020**, 251, 112623. https://doi.org/10.1016/ j.compstruct.2020.112623

[27] S.B. Shi, L.J. Li, J. Liang, S. Tang, *Int. J. Heat Mass Tran.* **2016***,* 102 (11), 1190-1198. https://doi.org/10.1016/j.ijheatmass transfer.2016.06.085

[28] J. Lachaud, J.B. Scoggins, T.E. Magin, M.G. Meyer, N.N. Mansour, *Int. J. Heat Mass Tran.* **2017***,* 108, 1406-1417. https://doi.org/10.1016/j.ijheatmasstransfer.2016.11.067

[29] B.K. Bessire, T.K. Minton, *ACS Appl. Mater. Inter.* **2017**, 9(25), 21422-21437. https://doi.org/10.1021/acsami.7b03919.

[30] H.K. Tran, C.E. Johnson, D.J. Rasky, F.C.L. Hui, M. Hsu, T. Chen, Y.K. Chen, D.

Paragas, L. Kobayashi, *NASA Tech. Memo.* **1997**, 110440, 1–69.

[31] Material properties database web edition version 4, National Aeronautics Space Administration. https://tpsx.arc.nasa.gov/, **2021**.

[32] J. Marschall, M. Cox, *J. Thermophys. Heat. Tr.* **1999**, 13(3), 382-384. https://doi.org/10.2514/2.6451